



**HAL**  
open science

# How thermally efficient are chaotic advection mixers? An experimental assessment

S.A. Bahrani, L. Humberset, R. Osipian, L. Royon, K. Azzouz, A. Bontemps

► **To cite this version:**

S.A. Bahrani, L. Humberset, R. Osipian, L. Royon, K. Azzouz, et al.. How thermally efficient are chaotic advection mixers? An experimental assessment. *International Journal of Thermal Sciences*, 2019, 145, 10.1016/j.ijthermalsci.2019.106046 . hal-03314813

**HAL Id: hal-03314813**

**<https://hal.science/hal-03314813>**

Submitted on 20 Jul 2022

**HAL** is a multi-disciplinary open access archive for the deposit and dissemination of scientific research documents, whether they are published or not. The documents may come from teaching and research institutions in France or abroad, or from public or private research centers.

L'archive ouverte pluridisciplinaire **HAL**, est destinée au dépôt et à la diffusion de documents scientifiques de niveau recherche, publiés ou non, émanant des établissements d'enseignement et de recherche français ou étrangers, des laboratoires publics ou privés.



Distributed under a Creative Commons Attribution - NonCommercial 4.0 International License

# How thermally efficient are chaotic advection mixers ? An experimental assessment.

S. Amir Bahrani<sup>a,b</sup>, Luc Humberset<sup>b,c</sup>, Rémy Osipian<sup>a</sup>, Laurent Royon<sup>b</sup>, Kamel Azzouz<sup>d</sup>, André Bontemps<sup>b</sup>

<sup>a</sup> *Université Paris Diderot, Sorbonne Paris Cité, MSC, UMR 7057 CNRS, 75013, Paris, France.*

<sup>b</sup> *Université Paris Diderot, Sorbonne Paris Cité, LIED, UMR 8236 CNRS, 75013, Paris, France.*

<sup>c</sup> *Ecole Normale Supérieure Paris-Saclay, Université Paris-Saclay, Cachan, France.*

<sup>d</sup> *Valeo Thermal Systems, 78321 La Verrière, France.*

---

## Abstract

Chaotic Laminar Mixers (CLMs) are static mixers whose concept uses chaotic advection based on baker's transformation. The present work is an attempt to study the CLMs from the viewpoint of heat transfer efficiency and global energy efficiency, and to compare the CLMs with helical heat exchangers. The influence of the number of bends and of the orientation of curvature planes was studied to bring out the role of regular and alternate Dean flow. An experimental investigation using water as inner hot fluid was carried out. It is shown that for the studied range of Reynolds numbers (100-2000), CLMs have a heat transfer efficiency two-times better than helical heat exchangers. However taking into account pressure losses, helical exchangers have better global energy efficiency than CLMs. For laminar flows, CLMs might be good heat exchangers when only mixing and heat transfer are the main requests.

*Keywords:* Chaotic advection, Heat transfer, Friction factor, Enhancement techniques, Energy efficiency.

---

## 1. Introduction

The efficiency of convective heat transfer with a flow in laminar regime is a major concern in industrial applications due to fluid physical properties (high viscosities), mechanical behavior (velocity profile, no fluid mixing) and device geometry (mini and microfluidic devices). In such systems, in the absence of a turbulent flow regime, heat transfer between the fluid and the wall occurs by molecular diffusion. In order to increase the heat and mass flow rate, several means can be used. It is usual to distinguish two types of enhancement techniques, passive or active [1, 2].

Passive techniques are those which do not necessitate an external energy source other than the energy

---

*Email address:* [seyed-amir.bahrani@univ-paris-diderot.fr](mailto:seyed-amir.bahrani@univ-paris-diderot.fr) (S. Amir Bahrani)

9 needed to circulate the fluids through the heat exchanger. In active techniques an external energy source  
10 is needed to modify the main flow. These last techniques penalize the global performance of a system  
11 because of the added energy cost. Many articles have been devoted to describe and analyze the most  
12 used techniques [3, 4, 5, 6, 7, 8, 9]

13 In passive techniques, the heat transfer rate can be improved in creating some disturbance in the fluid  
14 flow. However, this can induce a significant increase of the pumping power and finally of the pumping  
15 cost[6, 2]. To achieve the desired heat transfer rate at an economic pumping power, several techniques  
16 have been proposed. Several types of device have been implemented to create an extension of the heat  
17 transfer surface and/or to provoke some flow modification. In laminar regime the heat transfer coefficient  
18 is very large at the entrance of ducts and decreases with the increasing distance down to the final value  
19 for fully developed flow [10]. Flow inserts like fins or ribs interrupts this development and acts as a new  
20 entrance thus increasing the local heat transfer coefficient. Another way is to generate a secondary flow  
21 to mix the stream lines and/or to drive the core flow to the walls. Such a secondary flow can be produced  
22 by modifying the channel geometry in creating secondary channels to induce mixing [7] or in combining  
23 secondary channels and ribs [11]. This secondary flow also can appear by modifying the channel cross  
24 section [5] for example in making successive alternating wall deformations of the internal and external  
25 walls of an annular heat exchanger [12]. Another technique is to insert vortex generators which can take  
26 various cross-sectional shapes and forms such as protrusions, wings, inclined blocks, winglets, fins, and  
27 ribs[13, 14, 15, 16]. Secondary flows can also be produced in changing the cross section orientation for  
28 non-circular channels and heat transfer improvement has been observed[17, 18]. In their review, Ghani  
29 et al. [3] have underlined the role of two phenomena namely Dean vortices and chaotic advection. In  
30 this paper, in order to increase the heat transfer coefficient, we are particularly interested in a passive  
31 technique by using a phenomenon known as chaotic advection. In curved pipes, due to the secondary  
32 flow generated by centrifugal forces (see figure 1), transverse displacements of fluid particles are provoked  
33 and consequently the axial flow decreases leading to fluid mixing [19]. The Dean roll-cells, formed in the  
34 secondary flow, act as internal agitators which homogenize the flow. This mixing process is improved in  
35 separating the flow in two or several parts and in mixing them again together after. This is produced  
36 by the physical realization of a mathematical transformation known as the “baker’s transformation”.  
37 A practical realization of this transformation, which allows the exchange surface to be maximized in a

38 laminar regime, is the split and recombine (SAR) exchanger/mixer (called here Chaotic Laminar Mixers  
39 CLM). This geometry has been proposed for the first time by Gray et al. [20] and Chen & Meiners [21].  
40 The CLM concept is based on passive division of the flow, then a rotation in a curved pipe of opposite  
41 chirality and finally recombination for stretching and squeezing following the baker's transformation.  
42 From a Lagrangian point of view, the chaos can be quantified using the Lyapunov Exponent (LE). As  
43 mentioned by Carrière [22] the value obtained for the Lyapunov exponent is very close to the theoretical  
44 value of  $\ln 2$  predicted by the baker's map.

45 This specific flow regime was first introduced by Aref [23] and then received considerable attention for  
46 mixing [24, 25, 26] and heat transfer [27, 28, 29] applications. The enhancement of transport phenomena  
47 by means of chaotic advection in a twisted curved channel has been experimentally shown by Peerhossaini  
48 et al. [29]. Recently, Creyssels et al. [30] presented, numerically and experimentally, the influence of  
49 chaotic advection on heat transfer in a multi-level laminating mixer (MLLM). The MLLM is composed  
50 of 8 successive elements with the geometry early proposed by Gray et al.[20]. The authors reported  
51 that the Nusselt number averaged over each basic element forming the MLLM remains approximately  
52 constant whatever the element location, a behavior which relates to the cutting/stacking mechanism.

53 Anxionnaz-Minvielle et al.[27] experimentally compared the performances of the Gray's and Chen's  
54 exchanger-mixer to a plate-type heat exchanger/reactor with a corrugated pattern. The authors men-  
55 tioned that the more viscous the fluid, the more the energy efficiency of the SAR design increases  
56 compared to the corrugated design because of the balance between advection and diffusion mechanisms.  
57 A large increase in the internal convective heat transfer coefficient for the chaotic geometries compared  
58 to the straight tube is reported by Castelain et al. [28] in the bipolar plates for PEM fuel cells.

59 Consequently, a comparative study by Raynal & Gence [31] reported that the mixing in globally  
60 chaotic Stokes flow is more efficient than turbulent mixing in considering the energy dissipated by the  
61 mixing time.

62 The aim of the present study is to experimentally investigate the enhancement of heat transfer  
63 induced by chaotic advection in heat exchanger-mixers. In the present work, we propose two new CLM  
64 geometries alongside with the two classical geometries of Gray and Chen. We particularly focus on the  
65 effects of pipe curvature, number of bends and pipe orientations. In this context a quantitative study of  
66 the role of regular and alternated Dean flow, through four configurations of CLMs, has been performed

67 to investigate the enhancement of heat transfer.

68 A systematic comparison has been carried out with helical heat exchangers, which are commonly  
69 used in industry, in considering the same exchange surface. We have defined power-law correlations  
70 in the form of  $Nu = aPe^b$ . The pressure drop has been determined allowing us to calculate the Per-  
71 formance Evaluation Criterion (PEC) in order to assess the thermal-hydraulic performances. Together  
72 with thermal performance, the PEC was used to determine advantages and disadvantages of chaotic heat  
73 exchangers compared to helical heat exchangers.

74 The paper is organized as follows: Sec. 2 is devoted to a presentation of the chaotic advection.  
75 The experimental set-up, the different geometry of CLMs and of helical heat exchangers as well as the  
76 experimental procedure and measurements are described in sec. 3. The methodology used to obtain the  
77 convective heat transfer coefficient and pressure drop is presented in sec. 4. In sec. 5 we firstly propose  
78 to compare heat transfer performance of one of our CLMs with the same geometry as Creyssels et al.  
79 [30]. In this section are presented the experimental results for the different configurations of CLMs with  
80 comparison with two helical heat exchangers. Finally, Sec. 6 is devoted to a concluding discussion.

## 81 **2. Chaotic advection**

### 82 *2.1. Dean vortices*

83 If a fluid is moving along a curved pipe, two opposed forces apply on fluid particles perpendicularly of  
84 the direction of the main flow: centrifugal force due to the pipe curvature and force generated by pressure  
85 gradient. By naming "inner wall" (*iw*) the closest wall from the center of curvature and "outer wall" (*ow*)  
86 the farthest from this center (Figure 1), centrifugal force acts following the direction from inner wall to  
87 outer wall whereas pressure force acts on the opposite direction. On the median plane, centrifugal force  
88 gets the largest of pressure force thus fluid particles move towards outer wall. Particles movement slows  
89 down close to outer wall because of viscous forces. To insure momentum conservation, fluid particles  
90 return towards inner wall going close of upper and lower walls where velocities are lower. At this location,  
91 pressure forces are higher than centrifugal forces. Thereby competition between centrifugal force and  
92 pressure force gives rise to a secondary motion superimposed on the primary flow, and this secondary  
93 motion is expected to appear as a pair of counter-rotating cells, which are called Dean vortices [19].

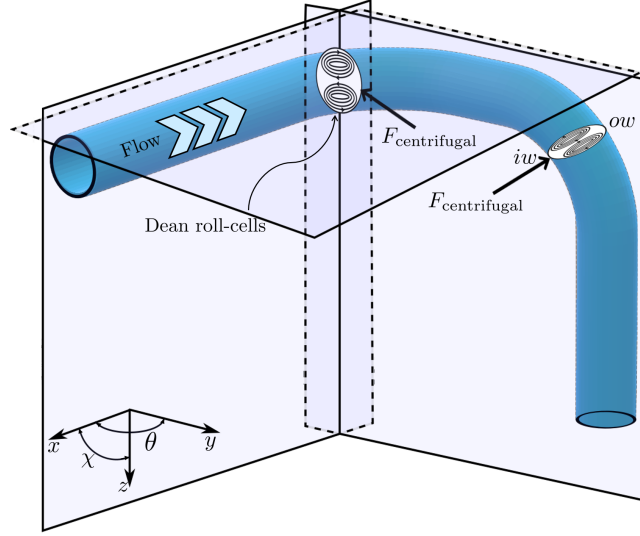


Figure 1: Basic unit of a curved pipe inducing Dean-roll cells.  $\theta$  is the angle between  $xz$  and  $yz$  planes and  $\chi$  is the angle between  $xy$  and  $yz$  planes (in this particular case  $\chi$  equal  $90^\circ$ ).

94 It is named after the british scientist W. R. Dean [19], who was the first to provide a theoretical  
 95 solution of the fluid motion through curved pipes for laminar flow by using a perturbation procedure  
 96 from a Poiseuille flow in a straight pipe to a flow in a pipe with very small curvature.

## 97 2.2. Alternated Dean flow and baker's transformation

98 As it is shown on figure 1, Dean vortices have an elliptic form. These vortices are not favorable for  
 99 mixing fluid particles in a quantitative way and they do not have a chaotic feature. To increase mixing,  
 100 one solution is to form a sequence of curved pipes by changing the orientation of the curvature plane of  
 101 each curved pipe. With each change of orientation of plane, positions of centers of Dean vortices and  
 102 their directions of rotation are modified (see figure 1). Fluid particle trajectories in this flow become  
 103 chaotic [32].

104 To better describe the effects from orientation of curvature plane, we call  $\chi$  the pitch angle between  
 105 2 successive curved pipes (figure 1). Jones et al (1989) [32] have studied effects of  $\chi$  angle on chaotic  
 106 advection in a twisted pipe. Their numerical experiments give qualitative guidelines on how to tune the  
 107 geometry of a pipe for maximum mixing efficiency. For  $\chi = 0^\circ$  and  $\chi = 180^\circ$ , that is a toroidal or helical  
 108 geometry, the flow is regular and mixing is low. For small deviations from  $\chi = 0^\circ$  or  $\chi = 90^\circ$ , regularity  
 109 of trajectories begins to decrease and a chaotic behavior is observed (moreover small deviations from  $\chi$   
 110  $= 0^\circ$  have a more profound impact on mixing than a comparable deviation from  $\chi = 180^\circ$ ). When  $\chi$

111 angle is  $90^\circ$ , the chaotic behaviour is at its maximum level thus maximum mixing is reached [29][32]. On  
 112 this experimental study, we focus on this specific geometry ( $\chi = 90^\circ$ ) and we use only the two values  $\chi$   
 113  $= 0^\circ$  and  $\chi = 90^\circ$  in order to compare their effects on heat transfer.

114 Chaotic advection by Dean flow appears at very low Reynolds number so in laminar flow what is very  
 115 interesting. Indeed, several heat transfers must be done at low Reynolds numbers as it is explained in  
 116 section 3 and they are limited by the laminar nature of the flow. Using Dean flow could lead to a homo-  
 117 geneous and efficient heat transfer for low Reynolds number application. Given its several advantages,  
 118 heat transfer by Dean flow has received a particular attention and has been subject to several studies,  
 119 especially experimental and numerical studies.

### 120 3. Experimental set-up and measurements

#### 121 3.1. Heat Exchanger-mixer: Design & Conception

122 The heat exchangers-mixers studied in this work either Chaotic Laminar Mixers (CLMs) or Helical  
 123 Heat Exchangers (HHEs) are made of copper alloy. The main geometrical characteristics are: inner  
 124 diameter  $d_i = 4.35$  mm and outer diameter  $d_o = 5.95$  mm.

##### 125 3.1.1. Chaotic Laminar Mixers (CLMs)

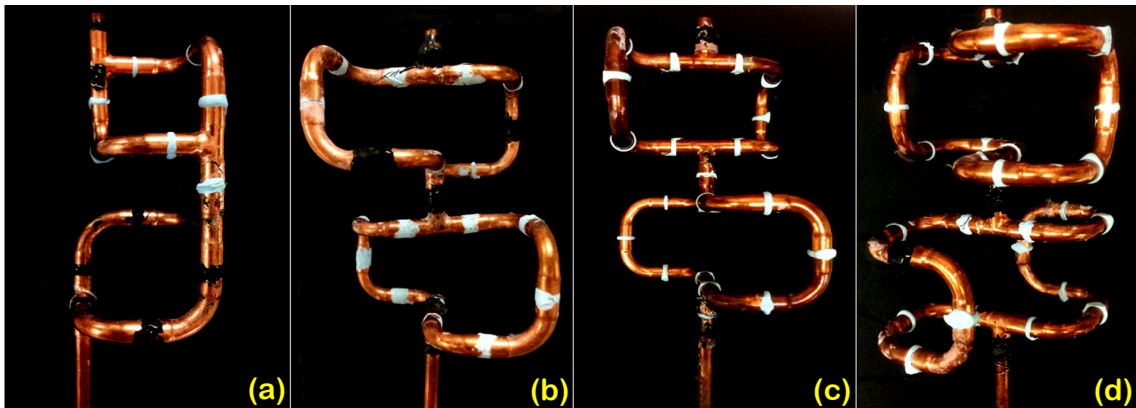


Figure 2: View of the four studied heat exchangers: (a) CLM<sub>1</sub> (b) CLM<sub>2</sub> (c) CLM<sub>3</sub> (d) CLM<sub>4</sub>.

126 Four CLMs ( $s = 1$  to  $4$ ) were constructed by joining copper alloy plumbing tubes, 90-degrees elbows  
 127 and T-couplers. For CLM<sub>1</sub>, two T-couplers and four 90-degrees elbows in copper are needed to build  
 128 the first part of the mixer. The second part has the same geometry than the first part but rotated of 90  
 129 degrees. Then the second part is added to the first part and the whole construction is the final mixer.

130 This geometry has been initially proposed by Chen and Meiners, (2004) [21]. As regards the CLM<sub>2</sub>,  
 131 introduced by Gray et al., (1999) [20], it followed the same realization technique but with two T-couplers  
 132 and eight 90-degrees elbows. CLM<sub>3</sub> has the same numbers of T-couplers and elbows than CLM<sub>2</sub> but  
 133 they are organized differently. Differences about organization of elbows are explained later. CLM<sub>4</sub> also  
 134 has the same numbers of T-couplers but has 12 elbows for each part. CLMs are shown on figure 2. The  
 135 total developed lengths are 43 cm for CLM<sub>1</sub>, 70 cm for CLM<sub>2</sub> and CLM<sub>3</sub> and 97 cm for CLM<sub>4</sub>. These  
 136 developed lengths were all experimentally and geometrically determined. Experimentally, by measuring  
 137 the volume of the water contained in each CLM and geometrically, by measuring the surface of the CLM  
 138 and deducting an equivalent developed length.

139 On figure 3, one can find the sequences of elbows of a branch for each CLM. Between 2 elbows, pitch  
 140 angle  $\chi$  has been noted in order to represent organization differences between CLMs. Only two values  
 141 of  $\chi$  are possible in our construction  $\chi = 0^\circ$  or  $\chi = 90^\circ$ .  $\chi = 90^\circ$  corresponds to an Orientation of the  
 142 Curvature Plane (OCP) which is better for chaotic mixing than  $\chi = 0^\circ$ .

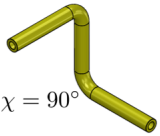
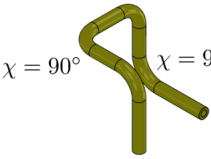
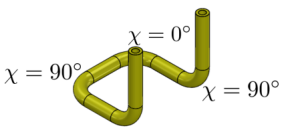
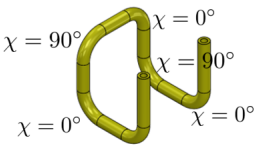
CLM <sub>1</sub>	 $\chi = 90^\circ$
CLM <sub>2</sub>	 $\chi = 90^\circ$ $\chi = 90^\circ$
CLM <sub>3</sub>	 $\chi = 90^\circ$ $\chi = 0^\circ$ $\chi = 90^\circ$
CLM <sub>4</sub>	 $\chi = 90^\circ$ $\chi = 0^\circ$ $\chi = 90^\circ$ $\chi = 0^\circ$

Figure 3: Breakdown of elements in one branch of CLMs.

143 Two parameters are important for construction of a CLM, namely the number of elbows and the  
 144 number of OCPs. In one branch, CLM<sub>1</sub> owns 2 elbows and 1 OCP, 4 elbows and 3 OCPs for CLM<sub>2</sub>,  
 145 4 elbows and 2 OCPs for CLM<sub>3</sub> and 6 elbows and 2 OCPs for CLM<sub>4</sub> (see figure 3). The equivalent  
 146 length of each CLM, which will be used later for the calculus of Nusselt number, is important because it



147 allows normalizing each CLM. Equivalent length is different than total developed length because mass  
 148 flow separates in two inside the CLM so only one branch must be taken into account for calculus of  
 149 equivalent length. Demonstration of this purpose is shown on Appendix A.

150 Choices of CLMs' geometry have been made by the following reasoning. First, geometries of Chen and  
 151 Gray (respectively CLM<sub>1</sub> and CLM<sub>2</sub>) have been constructed because they are the two main geometries  
 152 in chaotic heat transfer. Then, we wanted to observe both effects of number of OCPs and number of  
 153 elbows. CLM<sub>3</sub> has been constructed because it has less OCP than CLM<sub>2</sub> with the same number of  
 154 elbows than CLM<sub>2</sub>, so by comparing CLM<sub>2</sub> and CLM<sub>3</sub>, effects of number of OCPs might be observed.  
 155 Therefore, CLM<sub>4</sub> has been constructed because it has less elbows than CLM<sub>3</sub> with the same number of  
 156 OCPs than CLM 3, so by comparing CLM<sub>3</sub> and CLM<sub>4</sub>, effects of number of elbows might be observed.

### 157 3.1.2. Helical Heat Exchangers (HHEs)

158 We have compared the four studied CLMs with two Helical Heat Exchangers (HHEs) (see Figure  
 159 4). They are often used in industry, so this comparison could inform us on the possibility to use CLMs  
 160 at large scale. They have the same developed length than CLM<sub>4</sub> (about 1 m) and the same global  
 161 size,  $H_0 = 14$  cm and  $d_i = 4.35$  mm, than CLMs. These constraints allow two possibilities for helical  
 162 geometry which one has a higher pitch. To link helical geometry with chaotic advection, one can say  
 163 helical geometry is composed of several elbows with pitch angle close to zero. Moreover, pitch angle of  
 164 helical exchanger 1 is higher than exchanger 2.

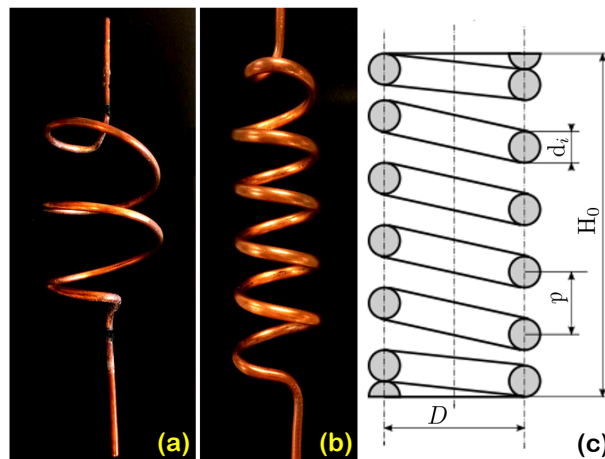


Figure 4: Helical Heat Exchangers: (a) HHE<sub>1</sub>:  $D = 10.5$  cm and  $p = 5.4$ , (b): HHE<sub>2</sub>:  $D = 5$  cm and  $p = 2.6$  and (c) Definition of geometrical parameters.

165 3.2. Experimental set-up

166 Inside the CLMs, and HHEs water circulated thanks to a pump and was heated by a constant-  
 167 temperature bath (Huber Ministat 125, Germany) fixed at 45 °C (see figure 5). Mass flow rate was  
 168 varied over a range from 0.5 to 5 (g/s) and was measured using a Coriolis mass flow controller (FIC,  
 169 mini Cori-Flow, Bronkhorst High-Tech B.V., Ruurlo, NL) providing accuracy of  $\pm 0.2\%$  of rate. A  
 170 pressure transmitter (AST 5100, USA) was used to measure the differential pressure between the input  
 171 and output of CLMs (with an uncertainty of  $\pm 1\%$ ).

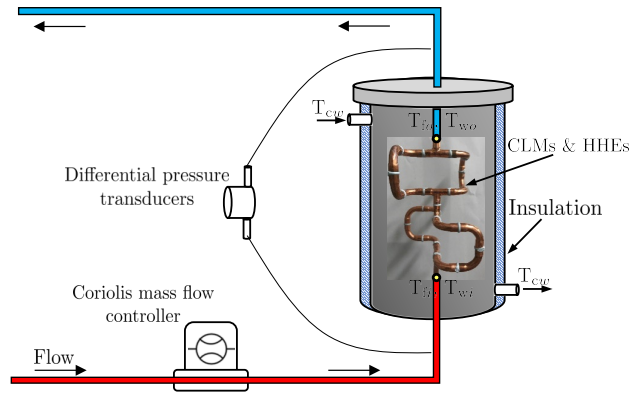


Figure 5: Schematic of the experimental loop.

172 Each CLMs was instrumented with 5 type K thermocouples: among them, two thermocouples ( $T_{fi}$   
 173 and  $T_{fo}$ ) measured the fluid temperature inside the CLM via a hole drilled in the wall of the copper,  
 174 and 2 thermocouples ( $T_{wi}$  and  $T_{wo}$ ) measured the temperature of the outer wall of the CLM. Subscript  
 175  $i$  indicated inlet whereas subscript  $o$  indicated outlet. The CLMs and HHEs described previously were  
 176 immersed in a cylindrical Plexiglas tube with dimensions of 20 cm diameter and 30 cm length. To  
 177 maintain the wall of the CLM at almost constant temperature of 20 °C, the cylindrical tube was filled with  
 178 water which the flow is ensured by an external cooler bath and pump (Huber Ministat 230, Germany).  
 179 Temperature of cold water was measured with type K thermocouples and practically no temperature  
 180 drift was observed during the recording time, despite the heat transfer with the CLM. Temperature  
 181 data were acquired every three seconds and sent to a computer by an acquisition data system (Keithley  
 182 Integra series 2700) with an accuracy of 0.2 °C. To determine this accuracy, all thermocouples have been  
 183 immersed inside a cold bath of 20 °C and the temperature data of all thermocouples varied no more  
 184 than 0.3 °C.

185 3.3. *Experimental procedure and measurements*

186 For each experiment, we have measured the several quantities as presented on figure 6. Measurements  
187 were carried out when a stationary state was reached. To have accurate values and to reduce uncertainties,  
188 we have recorded measurements on a long period, at least 10 times the dynamical period time. Then  
189 we have done a data average during the stationary state. From all these measurements we have deduced  
190 parameters of interest. Water properties like density or viscosity depends on water temperature. Because  
191 temperature water flowing in the heat exchanger decreases along the exchanger, we have fixed a reference  
192 for simplification reasons. For each experiment, we have chosen inlet temperature to determine water  
193 properties inside the exchanger.

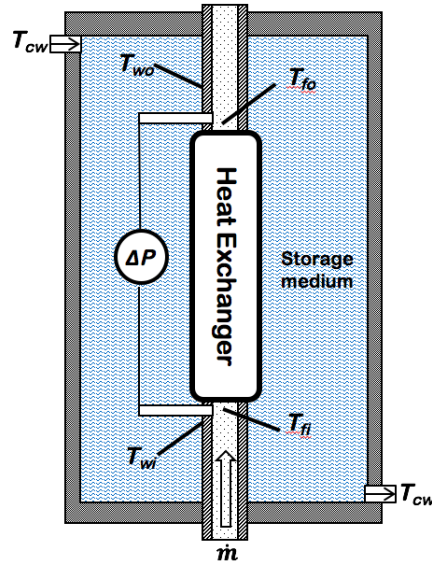


Figure 6: Summary of measured quantities in the test section.

194 During experiments it has been noted that the wall temperatures  $T_{wi}$  and  $T_{wo}$  were approximately  
195 constant ( $\pm 0.2$  °C). To deduce the useful quantities we have assumed that  $T_{wi} = T_{wo} = T_w$ .

196 **4. Data reduction**

197 *4.1. Heat transfer*

198 The heat flow rate  $\dot{Q}$  was determined from the measured mass flow rate  $\dot{m}$  and the inlet and outlet  
199 temperatures of the fluid  $T_{fi}$ ,  $T_{fo}$  inside the heat exchanger:

$$\dot{Q} = \dot{m}C_p(T_{fi} - T_{fo}) \quad (1)$$

200 From the heat flow rate, the internal heat transfer coefficient  $h$  between the fluid and the wall, can  
 201 be derived from the expression:

$$\dot{Q} = hA \left( \frac{T_{fi} - T_{fo}}{\ln \left( \frac{T_{fi} - T_w}{T_{fo} - T_w} \right)} \right) \quad (2)$$

202  $A$  being the heat exchange surface area.

203 In CLMs, a problem can raise due to division of the main flow in two parts followed by remixing:  
 204 what mass flow rates and what heat exchange surface areas must be used? As shown in the Appendix A,  
 205 we can use the total mass flow rate and we can consider that the heat exchange surface area is the area  
 206 of a single tube with  $d_i$  diameter and  $L$  length and we obtain  $A = \pi d_i L$ . The heat transfer coefficient  
 207 can be written as a function of the Nusselt number  $Nu$  by:

$$h = \frac{Nu\lambda}{d_i} \quad (3)$$

208 With the expression of the heat transfer rate and, introducing the Reynolds and Prandtl numbers

$$Re = \frac{\rho V d_i}{\mu} \quad (4)$$

$$Pr = \frac{\mu C_p}{\lambda} \quad (5)$$

209 where  $\rho$  and  $\mu$  are the mass density and the dynamic viscosity of the fluid respectively.  $V$  is the mean  
 210 flow velocity. Introducing the Péclet number  $Pe$ , which is defined by:

$$Pe = RePr \quad (6)$$

211 the Nusselt number becomes:

$$Nu = \frac{d_i Pe}{4L_{eq}} \ln \left( \frac{T_{fi} - T_w}{T_{fo} - T_w} \right) \quad (7)$$

212 where  $L_{eq}$  is the developed length of the CLMs. This number was extracted from measurements.

213 *4.2. Pressure drop*

214 The pressure drop inside the pipes was directly measured and compared with the Darcy-Weisbach  
215 equation:

$$\Delta p = \Lambda \frac{L_{eq}}{d_i} \rho \frac{V^2}{2} \quad (8)$$

216 where  $\Lambda$  is the Darcy friction factor. The  $\Lambda$  factor was extracted from measurements and compared  
217 to the Poiseuille law obtained for laminar flow in a smooth tube:

$$\Lambda = \frac{64}{Re} \quad (9)$$

218 **5. Results and discussions**

219 *5.1. Heat transfer*

220 *5.1.1. Nusselt number evolution*

221 Nusselt numbers have been deduced using formula 7. As an example, we give on figure 7 values of  $Nu$   
222 as a function of  $Pe$  obtained with CLM<sub>2</sub> based on Gray geometry. For each measurement error bars are  
223 shown. The uncertainty has been determined with the method of error propagation described in annex  
224 B. On the same figure these results have been compared with those of Creyssels et al. [30] obtained with  
225 an analogue geometry. It is seen that results are very close especially when  $Pe \geq 1700$ . Both results  
226 follow a comparable variation of the form  $Nu \sim Pe^{1/2}$ . We notice that the Creyssel's results are the  
227 same as ours for their second element and lower for the first element.

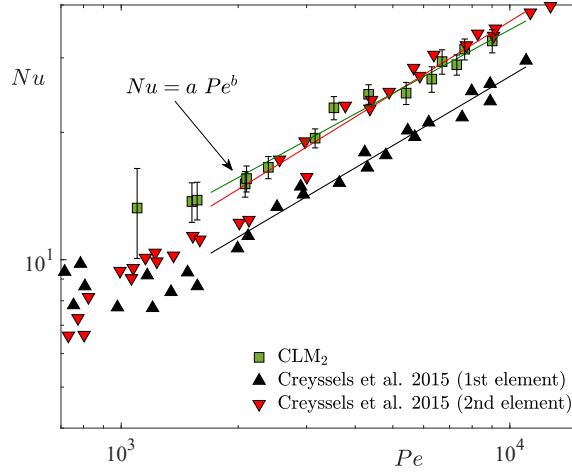


Figure 7: Variation of the Nusselt number as a function of the Péclet number for CLM<sub>2</sub>. Comparison with Creyssel's results.

228 By fitting the experimental points with straight lines in logarithmic coordinates we can find out  
 229 correlations of the form  $Nu = a Pe^b$ . The obtained values are given in Table 1.

CLMs	$a$	$b$
CLM <sub>2</sub>	0.35	0.5
Creyssel first element	0.1826	0.543
Creyssel second element	0.19	0.568

Table 1: Coefficients  $a$  and  $b$  obtained from the correlation  $Nu = a Pe^b$ .

### 230 5.1.2. Thermal comparison of CLMs

231 Due to different equivalent lengths  $L_{eq}$  it is difficult to compare directly the Nusselt numbers of the  
 232 four CLMs. We have chosen to rescale them by the Nusselt number of a straight pipe which would have  
 233 the same equivalent length. Nusselt number evolution for a straight pipe with constant wall temperature  
 234 is known as the Graetz's problem [33]. For a straight pipe of length  $L_{eq}$  and a flow characterized by the  
 235 Péclet number  $Pe$ , the Nusselt number for an established dynamical regime is given by

$$Nu_{\text{straight pipe}} = 3.66 + \frac{0.127}{L^* + 0.0635L^{*1/3}} \quad (10)$$

236 where

$$L^* = \frac{2L_{eq}}{Pe d_i} \quad (11)$$

So, we define a reduced Nusselt number by

$$Nu_{\text{red}} = \frac{Nu}{Nu_{\text{straight pipe}}} \quad (12)$$

The reduced Nusselt numbers  $Nu_{\text{red}}$  are presented on Figures 8a and 8b as a function of  $Pe$  and  $Re$

respectively.

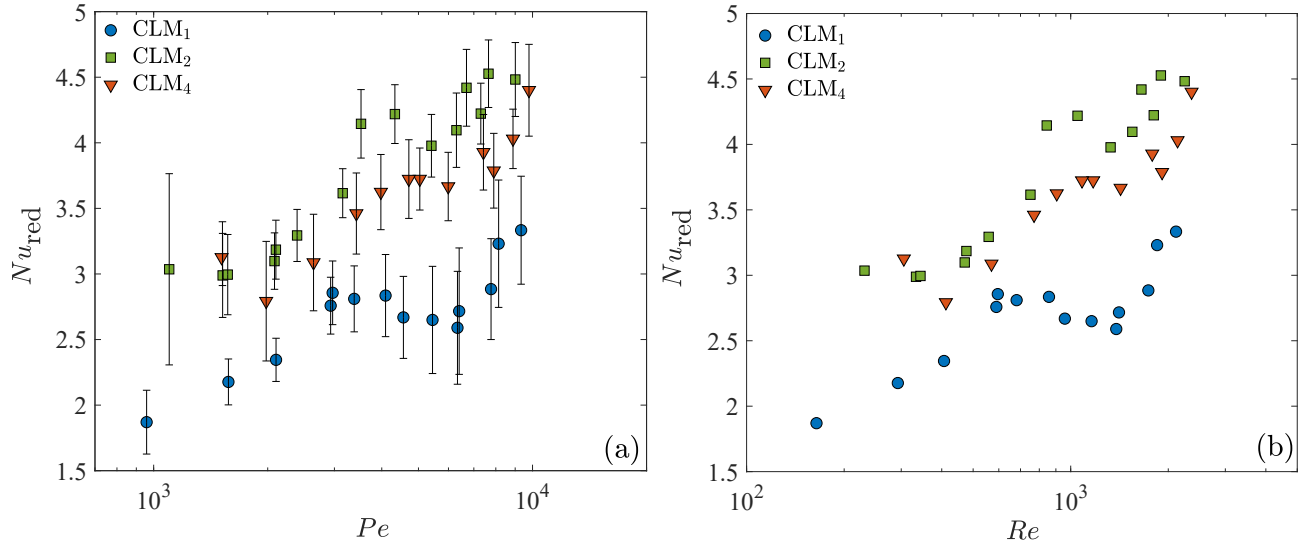


Figure 8: Variation of the reduced Nusselt number as a function of Péclet and Reynolds numbers.

Several comments can be done: Firstly, it is observed that the shown experimental points are clearly

distinct from one CLM to another. For each CLM they are mainly outside the range of error bars of

its neighboring. Second, compared to a straight tube with the same exchange surface area, the heat

transfer enhancement reaches more than 200 % for CLM<sub>1</sub> and more than 400% for CLM<sub>2, 3</sub> and 4. One

of the reasons of the heat transfer enhancement in the CLMs is the chaotic effect of the flow. Indeed,

the flow paths are not parallel as in a straight tube but rapidly diverge, which results that hot particles

located in the center region move in the cold region close to the wall. Consequently, the heat transfer is

enhanced and the Nusselt number is increased.

Third, CLM<sub>2</sub> seems to be more performing than CLM<sub>3</sub> and 4, and these three CLMs are more per-

forming than CLM<sub>1</sub>. Knowing differences of geometries between CLMs (see figure 3), one can assume

that it is a consequence of the number of elbows and number of OCPs. CLM<sub>1</sub> and CLM<sub>2</sub> have the

same organization sequence (all  $\chi$  angles equal to  $90^\circ$ ), thus an increase of elbow number leads to more

alternating Dean vortices and a better heat transfer. CLM<sub>1</sub> has only one OCP, CLM<sub>3</sub> and 4 have 2 OCPs

253 and CLM<sub>2</sub> has 3; looking at  $Nu_{\text{red}}$  results, one can note that OCP is clearly beneficial for heat transfer  
 254 and mixing. Moreover CLM<sub>3</sub> and CLM<sub>4</sub> have the same number of OCPs but not the same number of  
 255 elbows and not the same organization, and one note that heat transfer is quite similar.

256 Experimental results exhibit a kind of plateau for all CLMs. CLM<sub>2, 3 and 4</sub> exhibit a plateau for  
 257  $Pe = 1700$  or  $Re = 300$ , whereas for CLM<sub>3</sub>, a large plateau is observed when  $3000 \leq Pe \leq 6000$  or  $500$   
 258  $\leq Re \leq 1200$ . No physical interpretation is known to this day in order to explain these plateaus apart  
 259 from the fact that there is clearly some reorganization of the flow and the temperature fields. At last, no  
 260 significant changes are noted between  $Re$  representation and  $Pe$  representation. Indeed, Prandtl number  
 261  $Pr$  is quite constant for all experiments (close to 7). For next results, only  $Re$  representation will be  
 262 used.

### 263 5.1.3. Thermal comparison of CLMs with helical heat exchangers

264 As CLM<sub>2</sub> seems to be the most performing we only have compared its results with the two previously  
 265 described helical heat exchangers. In Figure 9 are reported the Nusselt number values for the two used  
 266 helical heat exchangers and no significant difference is observed between the two heat exchangers up to  
 267  $Re \approx 1500$  (see Fig. 9) but beyond this value a maximum is seen for the heat exchanger which has the  
 268 most number of spires. These values have been compared to those given by the Manlapaz and Churchill  
 269 (MC) correlation [34]. It appears that up to Reynolds numbers of about 1000 the obtained values are  
 270 very close to those of MC due to the fact that their correlation is essentially based upon low Reynolds  
 271 number values ( $Re \leq 1000$ ). We note a difference beyond this value, our results tending to a maximum.

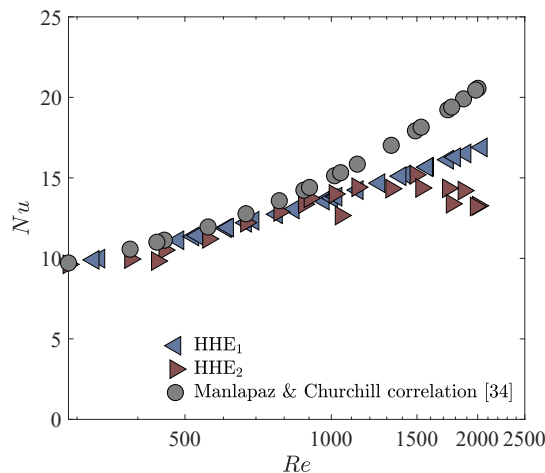


Figure 9: Evolution of the Nusselt numbers of the two studied helical heat exchangers with the Reynolds number. Comparison with the Manlapaz and Churchill correlation [34].



272 The reduced Nusselt numbers also have been calculated and we observe Fig. 10 that helical heat  
 273 exchangers have a Nusselt number greater than 1 as expected. They have been compared with those of  
 274 the CLM<sub>2</sub> heat exchanger which are the highest values among the CLMs. The interesting point is that  
 275 CLM<sub>2</sub> has a higher Nusselt number than both helical heat exchangers. CLMs might be a better choice  
 276 than HHE to improve heat transfer.

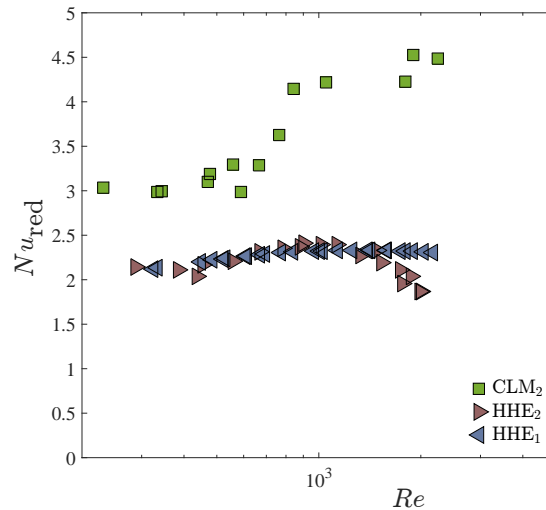


Figure 10: Comparison of the reduced Nusselt number of Helical Heat Exchangers with CLM<sub>2</sub>.

## 277 5.2. Pressure drop

### 278 5.2.1. Comparison of CLMs pressure drop

279 The pressure drop along the heat exchangers is particularly important to examine the mechanical  
 280 power needed for the requested flow rate. From pressure drop measurements and formula 8 the Darcy  
 281 coefficient  $\Lambda$  has been determined. It has been reported in figure 11a for all CLMs together with the  
 282 Poiseuille classical value valid for established laminar regime in smooth tubes (equation 9).

283 The  $\Lambda$  values seem to be linked to the number of (elbows plus OCP) even though the gap between  
 284 them is small. However, all values are about ten times those of a smooth straight tube. The presence of  
 285 elbows, split and recombination structures causes singular losses which explain the huge pressure drop  
 286 observed. However, the CLMs pressure drop obeys roughly to the same power law as a straight tube  
 287 ( $\text{Re}^{-1}$ ) in laminar regime.

### 288 5.2.2. Comparison of CLMs pressure drop with helical heat exchangers

289 On Figure 11b are reported Darcy coefficient values for the two HHEs together with those obtained  
 290 with CLM<sub>2</sub> which is the most thermally performing. The Darcy coefficient is lower for HHEs than for

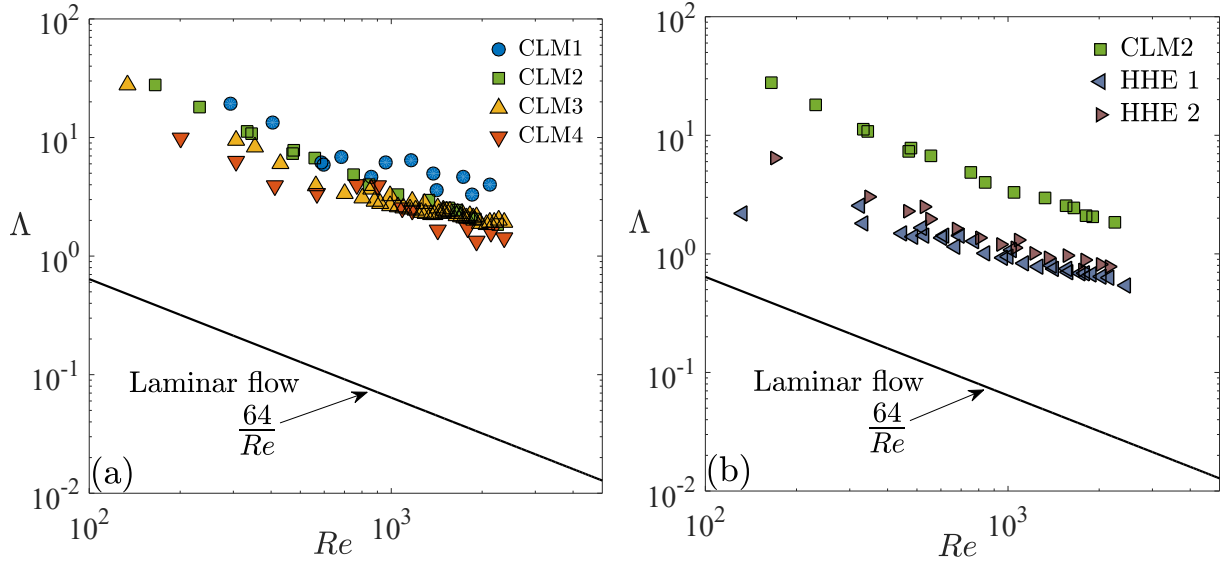


Figure 11: Darcy coefficients in function of the Reynolds number (a) for CLMs (b) comparison of CLM<sub>2</sub> with Helical Heat Exchangers.

CLMs due to absence of recombination structures. It must be remarked that, the flow regime is laminar, the Reynolds number being lower than the critical Reynolds,  $Re_{crit}$ . According to different authors, this critical Reynolds number is between 7000 and 7300 for HHE<sub>1</sub> and between 8700 and 9100 for HHE<sub>2</sub> [35, 36].

### 5.3. Performance Evaluation Criterion (PEC)

As already employed in many studies [37, 38] we have used the Performance Energy Criterion, (PEC) which is based on an energy global approach. It is defined as the ratio of the transferred heat flow rate to the required pumping power for the fluid circulation in the test section.

$$PEC = \frac{\text{Heat flow rate}}{\text{Pumping power}} = \frac{\dot{m}c_p(T_{fi} - T_{fo})}{Q_v \Delta p} \quad (13)$$

$Q_v$  being the volume flow rate. If the transferred thermal power is greater than the mechanical power,  $PEC > 1$ .

From the data measurements, PEC was determined for CLMs and HHEs. As well as for the Nusselt number we have rescaled the actual PEC with PEC of a straight pipe of equivalent length, delivering

303 the same thermal power. We have noted  $\delta$  this ratio:

$$\delta = \frac{PEC}{PEC_{\text{Straight pipe}}} \quad (14)$$

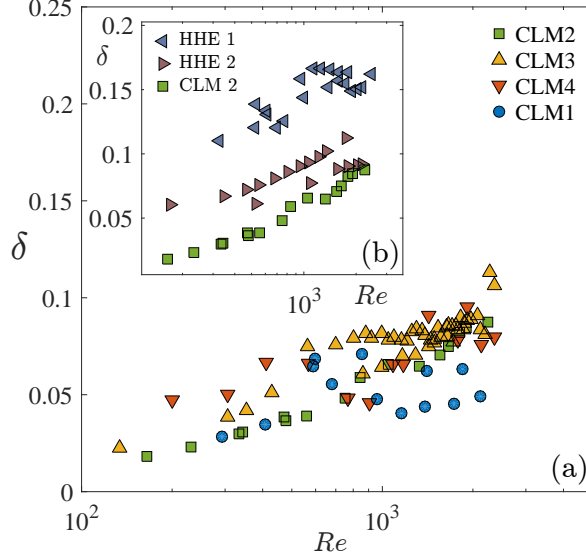


Figure 12: Evolution of the ratio  $\delta$  in function of the Reynolds number. (a) for CLMs (b) for HHEs compared to CLM<sub>2</sub>.

304 In Figure 12a, are presented PECs for the four CLMs. It is observed that the PECs have a very  
 305 low value (from 0.01 to about 0.12) due to the high value of the pressure drop. We note that the PECs  
 306 increase regularly with  $Re$ . The comparison with helical heat exchangers is shown in the inset of Figure  
 307 12b. It is clearly seen that the helical heat exchangers have a better PEC than CLMs. On a global  
 308 energy approach, helical heat exchangers have a better energy efficiency than CLMs.

## 309 6. Conclusion

310 To enhance heat transfer at low Reynolds, we have used the chaotic advection based on baker's  
 311 transformation. This latter finds its origin through the Dean flow and the split and-recombination  
 312 structure.

313 To observe effects of Dean flow on heat transfer, we have constructed different Chaotic Laminar  
 314 Mixers (CLMs) with different geometrical characteristics. Number of elbows has been modified as well  
 315 as number of OCPs representing organization and structure of the CLMs: CLM<sub>1</sub> has only one OCP,  
 316 CLMs<sub>3</sub> and 4 have 2 OCPs and CLM<sub>2</sub> has 3. Results show that heat transfer is improved when number

317 of OCPs increases while the pressure drop is quite the same. Then, we have compared our CLMs  
 318 with helical exchangers in order to determine if our CLMs could be used in a global energy approach.  
 319 CLMs have two-times better heat transfer than helical exchangers. Concerning pressure drops, CLMs  
 320 are about three-times less efficient than helical exchangers. This implies that helical exchangers have a  
 321 better efficiency than CLMs. This efficiency has been quantified through a Performance Energy Criterion  
 322 (PEC).

323 As a consequence, CLMs can be recommended in the case where mixing and heat transfer only are  
 324 the main specification requests. Moreover, between CLMs, CLM<sub>2</sub> is the best solution for mixing at  
 325 industrial scale. Indeed, for a higher quality mixing, CLM<sub>2</sub> has less elbows than CLM<sub>3</sub> and 4, so that  
 326 implies a diminution of costs.

### 327 Appendix A. Calculation of the Nusselt number in the studied Chaotic Heat Exchangers

328 In the expression of the Nusselt number given in formula 7 we have used the total mass flow rate and  
 329 an equivalent heat exchange area to calculate the Péclet number. An elementary unit of flow separation  
 330 and remixing in a chaotic heat exchanger can be schematically represented on Figure A.13.

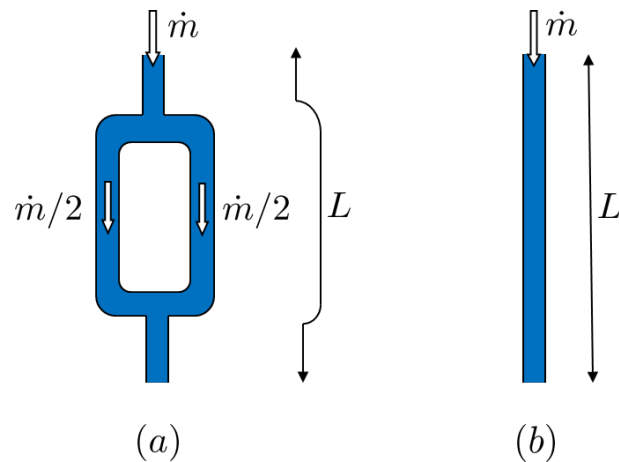


Figure A.13: (a) Flow paths in the first part of a unit of the chaotic heat exchanger (b) Simplified representation used to extract quantities of interest.

331 The heat exchanger consists of several units with two equivalent branches and its total length is  $L_t$ .  
 332 The equivalent length of a unit is  $L$ . Neglecting the straight part at the inlet and outlet, the Reynolds  
 333 number must be calculated with the  $\dot{m}/2$  mass flow rate in each branch.

334 The power transferred to (or from) the tube wall by (or from) the fluid in each branch  $j$  is (Figure

335 A.13a):

$$Q' = h' A'_j (\Delta T_{ml}) \quad (\text{A.1})$$

336 Where  $A'_j = \pi d_i L$  and where  $h'$  is calculated with the help of the Nusselt number which depends on  
337 a Reynolds number. The mean logarithmic difference is given by:

$$\Delta T_{ml} = \left( \frac{T_i - T_o}{\ln \left( \frac{T_i - T_w}{T_o - T_w} \right)} \right) \quad (\text{A.2})$$

338 Where  $T_i$  and  $T_o$  are the fluid temperatures at the inlet and the outlet of the unit respectively.

339 In one branch, the Reynolds number is:

$$Re' = \frac{2\dot{m}}{\pi d_i \mu} \quad (\text{A.3})$$

340 And the Nusselt number and the heat transfer coefficient become:

$$Nu' = \frac{Re' Pr d_i}{4L} \ln \left( \frac{T_i - T_w}{T_o - T_w} \right) \quad (\text{A.4})$$

$$h' = \frac{Nu' \lambda}{d_i} \quad (\text{A.5})$$

341 If  $\dot{m}$  is the total mass flow rate (at the heat exchanger inlet, for example), the total power transferred  
342 by the two branches is:

$$Q = 2Q' = 2h' A'_j (\Delta T_{ml}) \quad (\text{A.6})$$

343 Assuming that only one branch would be existing in which the whole flow circulates with the mass  
344 flow rate  $\dot{m}$ , in this unique branch the Reynolds number is:

$$Re = \frac{4\dot{m}}{\pi d_i \mu} = 2Re' \quad (\text{A.7})$$

345 The associate Nusselt number can be written:

$$Nu = \frac{Re Pr d_i}{4L} \ln \left( \frac{T_i - T_w}{T_o - T_w} \right) = 2Nu' \quad (\text{A.8})$$

346 Then, the heat transfer coefficient is:

$$h = \frac{Nu\lambda}{d_i} = 2h' \quad (\text{A.9})$$

347 Taking into account

$$Q = 2Q' = h\pi d_i L(\Delta T_{ml}) \quad (\text{A.10})$$

348 The Nusselt number deduced from the equation 7 can be used to determine the heat transfer coefficient.  
349

## 350 Appendix B. Measurement uncertainty

351 The estimation of the measurement uncertainty is based on the method of error propagation described  
352 by Moffat [39]. For a  $y$  function depending on  $N$  independent parameters, the uncertainty is given by:

$$\Delta y = \sqrt{\sum_{i=1}^N \left( \frac{\partial y}{\partial p_i} \Delta p_i \right)^2} \quad (\text{B.1})$$

353 Assuming that there is no error on the physical properties and on the geometrical parameters, from  
354 the following Nusselt expression:

$$Nu = \frac{RePrd_i}{4L_{eq}} \ln \left( \frac{T_{fi} - T_w}{T_{fo} - T_w} \right) \quad (\text{B.2})$$

355 We can write:

$$\Delta(Nu) = \sqrt{\left( \frac{\partial Nu}{\partial Re} \Delta Re \right)^2 + \left( \frac{\partial Nu}{\partial T_{fi}} \Delta T_{fi} \right)^2 + \left( \frac{\partial Nu}{\partial T_{fo}} \Delta T_{fo} \right)^2 + \left( \frac{\partial Nu}{\partial T_w} \Delta T_w \right)^2} \quad (\text{B.3})$$

## 356 References

- 357 [1] A. E. Bergles, R. M. Manglik, Current progress and new developments in enhanced heat and mass  
358 transfer, *J. Enhanced Heat Transfer* 20 (2013) 1–15.
- 359 [2] A. E. Bergles, Enhanced heat transfer: endless frontier, or mature and routine?, *J. Enhanced Heat*  
360 *Transfer* 6 (1999) 79–88.

- 361 [3] I. A. Ghani, N. A. C. Sidik, N. Kamaruzaman, Hydrothermal performance of microchannel heat  
362 sink: The effect of channel design, *Int. J. Heat Mass Tran.* 107 (2017) 21–44.
- 363 [4] L. Léal, M. Miscevic, P. Lavieille, M. Amokrane, F. Pigache, F. Topin, B. Nogarède, L. Tadrif,  
364 An overview of heat transfer enhancement methods and new perspectives: Focus on active methods  
365 using electroactive materials, *Int. J. Heat Mass Tran.* 61 (2013) 505–524.
- 366 [5] M. Siddique, A.-R. A. Khaled, N. I. Abdulhafiz, A. Y. Boukhary, Recent advances in heat transfer  
367 enhancements: A review report, *Int. J. Chem. Eng.* 2010 (2010) 1–28.
- 368 [6] A. Dewan, P. Mahanta, K. S. Raju, P. S. Kumar, Review of passive heat transfer augmentation  
369 techniques, *J. Power Energy* 218 (7) (2004) 509–527.
- 370 [7] M. E. Steinke, S. G. Kandlikar, Review of single-phase heat transfer enhancement techniques for  
371 application in microchannels, minichannels and microdevices, *Int. J. Heat Techn.* 22 (2004) 3–11.
- 372 [8] P. M. Ligrani, M. M. Oliveira, T. Blaskovich, Comparison of heat transfer augmentation techniques,  
373 *AIAA Journal* 41 (2003) 337–362.
- 374 [9] W. Q. Tao, Y. L. He, Q. W. Wang, Z. G. Qu, F. Q. Song, A unified analysis on enhancing single phase  
375 convective heat transfer with field synergy principle, *Int. J. Heat Mass Tran.* 45 (2002) 4871–4879.
- 376 [10] A. Bejan, *Convection heat transfer*, 2nd ed., John Wiley & Sons, Inc., New York, USA.
- 377 [11] I. A. Ghani, N. A. C. Sidik, R. Mamat, G. Najafi, T. L. Ken, Y. Asako, W. M. A. A. Japar,  
378 Heat transfer enhancement in microchannel heat sink using hybrid technique of ribs and secondary  
379 channels, *Int. J. Heat Mass Tran.* 114 (2017) 640–655.
- 380 [12] J.-A. Zambaux, J.-L. Harion, S. Russeil, P. Bouvier, The effect of successive alternating wall defor-  
381 mation on the performance of an annular heat exchanger, *Appl. Therm. Eng.* 90 (2015) 286–295.
- 382 [13] T. Lemenand, C. Habchi, D. D. Valle, H. Peerhossaini, Vorticity and convective heat transfer down-  
383 stream of a vortex generator, *Int. J of Therm. Sci.* 125 (2018) 342–349.
- 384 [14] G. Zhou, Z. Feng, Experimental investigations of heat transfer enhancement by plane and curved  
385 winglet type vortex generators with punched holes, *Int. J of Therm. Sci.* 78 (2014) 26–35.

- 386 [15] C. Habchi, J.-L. Harion, S. Russeil, D. Bougeard, F. Hachem, A. Elmarakbi, Chaotic mixing by  
387 longitudinal vorticity, *Chem. Eng. Sci.* 104 (2013) 439–450.
- 388 [16] C. Habchi, S. Russeil, D. Bougeard, J.-L. Harion, T. Lemenand, D. D. Valle, H. Peerhossaini,  
389 Enhancing heat transfer in vortex generator-type multifunctional heat exchangers, *Appl. Therm.*  
390 *Eng.* 38 (2012) 14–25.
- 391 [17] O. Keklikcioglu, V. Ozceyhan, Experimental investigation on heat transfer enhancement in a circular  
392 tube with equilateral triangle cross sectioned coiled-wire inserts, *Appl. Therm. Eng.* 131 (2018) 686–  
393 695.
- 394 [18] R. Filimonov, J. Sorvari, Numerical study on the effect of cross-section orientation on fluid flow  
395 and heat transfer in a periodic serpentine triangular microchannel, *Appl. Therm. Eng.* 125 (2017)  
396 366–376.
- 397 [19] W. R. Dean, Xvi. note on the motion of fluid in a curved pipe, *The London, Edinburgh, and Dublin*  
398 *Philosophical Magazine and Journal of Science* 4 (20) (1927) 208–223.
- 399 [20] B. Gray, D. Jaeggi, N. Mourlas, B. van Drie Novel interconnection technologies for integrated  
400 microfluidic systems1paper presented as part of the ssaw-98 workshop.1, *Sens. Actuator A-Phys.*  
401 77 (1) (1999) 57 – 65.
- 402 [21] H. Chen, J.-C. Meiners, Topologic mixing on a microfluidic chip, *Appl. Phys. Lett.* 84 (12) (2004)  
403 2193–2195.
- 404 [22] P. Carrière, On a three-dimensional implementation of the baker’s transformation, *Phys. Fluids*  
405 19 (11) (2007) 118110.
- 406 [23] H. Aref, Stirring by chaotic advection, *J. Fluid Mech.* 143 (1984) 1—21.
- 407 [24] Z. Habibi, M. Karami, M. Jarrahi, E. Shirani, H. Peerhossaini, Some observations on the spatiotem-  
408 poral orbits structure and heat transfer enhancement in pulsating flow, *Int. J of Therm. Sci.* 125  
409 (2018) 428–439.
- 410 [25] M. Jarrahi, C. Castelain, H. Peerhossaini, Mixing enhancement by pulsating chaotic advection,  
411 *Chem. Eng. Process.* 74 (2013) 1–13.



- 412 [26] B. Timité, C. Castelain, H. Peerhossaini, Mass transfer and mixing by pulsatile three-dimensional  
413 chaotic flow in alternating curved pipes, *Int. J. Heat Mass Tran.* 54 (17) (2011) 3933–3950.
- 414 [27] Z. Anxionnaz-Minvielle, P. Tochon, R. Couturier, C. Magallon, F. Théron, M. Cabassud, C. Gour-  
415 don, Implementation of ‘chaotic’ advection for viscous fluids in heat exchanger/reactors, *Chem. Eng.*  
416 *Process.* 113 (2017) 118–127.
- 417 [28] C. Castelain, Y. Lasbet, B. Auvity, H. Peerhossaini, Experimental study of the thermal performance  
418 of chaotic geometries for their use in pem fuel cells, *Int. J of Therm. Sci.* 101 (2016) 181–192.
- 419 [29] H. Peerhossaini, C. Castelain, Y. L. Guer, Heat exchanger design based on chaotic advection, *Exp.*  
420 *Therm. Fluid Sci.* 7 (4) (1993) 333–344.
- 421 [30] M. Creyssels, S. Prigent, Y. Zhou, X. Jianjin, C. Nicot, P. Carrière, Laminar heat transfer in the  
422 mllm static mixer, *Int. J. Heat Mass Tran.* 81 (2015) 774–783.
- 423 [31] F. Raynal, J.-N. Gence, Energy saving in chaotic laminar mixing, *Int. J. Heat Mass Tran.* 40 (14)  
424 (1997) 3267–3273.
- 425 [32] S. W. Jones, O. M. Thomas, H. Aref, Chaotic advection by laminar flow in a twisted pipe, *J. Fluid*  
426 *Mech.* 209 (1989) 335–357.
- 427 [33] L. Graetz, Ueber die wärmeleitungsfähigkeit von flüssigkeiten, *Annalen der Physik* 18 (1883) 79–94.
- 428 [34] R. L. Manlapaz, S. W. Churchill, Fully developed laminar convection from helical coil, *Chem. Eng.*  
429 *Commun.* 9 (1981) 185–200.
- 430 [35] H. Ito, Friction factors for turbulent flow in curved pipes, *J. Basic Eng.* 81 (1959) 123—132.
- 431 [36] E. F. Schmidt, Wärmeübergang und druckverlust in rohrschlangen, *Chemie Ingenieur Technik*  
432 39 (13) (1967) 781–789.
- 433 [37] A. E. Bergles, Recent developments in enhanced heat transfer, *Heat Mass Transfer.* 47 (2011) 1001–  
434 1008.
- 435 [38] A. E. Bergles, Survey and evaluation of techniques to augment convective heat and mass transfer,  
436 *Prog. Heat Mass Tran.* 1 (1969) 331–424.

<sup>437</sup> [39] R. J. Moffat, Describing the uncertainties in experimental results, *Exp. Therm. Fluid Sci.* 1 (1988)  
<sup>438</sup> 3–17.